International Journal of Thermophysics, Vol. 27, No. 3, May 2006 (© 2006)
DOI: 10.1007/s10765-006-0067-9

Measurements of the Thermal Conductivity and Thermal Diffusivity of Liquids. Part II: "Convective and Radiative Effects"[1]

B. Remy[2,3] and A. Degiovanni[2]

The second part (Part II) of this work is concerned with coupling in the transient regime of conduction with convection and radiation in the experimental bench developed and presented in Part I for the measurement of the thermal conductivity and thermal diffusivity of fluids by an impulse technique. The first section will analyze heat transfer in the liquid by conduction and convection. This will help to define the optimal extension of the measuring cell to reduce the influence of natural convection for the case of impulse heat flux stimulation. The second section is about coupled conductive–radiative heat transfer and will show how to deal with radiative effects in the problem of parameters estimation.

KEY WORDS: convection; coupled heat transfers; fluids; radiation; transient technique.

1. INTRODUCTION

The aim of this work is to implement an experimental bench for measurement of the thermal diffusivity and conductivity of liquids by a transient

[1] Paper presented at the Seventh Asian Thermophysical Properties Conference, August 23–28, 2004, Hefei and Huangshan, Anhui, P. R. China.

[2] L.E.M.T.A U.M.R-C.N.R.S 7563/E.N.S.E.M.–02, avenue de la Forêt de Haye, B.P 160, 54 504 Vandoeuvre-Lès-Nancy Cedex, France.

[3] To whom correspondence should be addressed. E-mail: benjamin.remy@ensem.inpl-nancy.fr

impulse technique. The measurement of the thermal conductivity of fluids is particularly difficult due to the presence of several coupled modes of heat transfer: conduction, convection and radiation, disturbed by the presence of solid boundaries that also take part in heat exchange. The first part of this work (Part I) allowed us — by a sensitivity study of the theoretical model and validation by experiments — to optimize, assuming purely conductive transfer, the parameters estimation procedure and to precisely define the main characteristics of the walls (thickness and thermophysical properties) to perform such a measurement. The aim of this second part (Part II) consists of studying the effects of convection and radiation in the transient regime. Some details will be given about end effects and conduction through the measuring cell walls.

2. CONVECTIVE HEAT TRANSFER

The vertical cylindrical geometry chosen for the measurement does not totally eliminate convection effects. To perform a good measurement, it is thus necessary to work in a regime called a "pseudo-conduction" regime, in which convection has no affect on heat transfer by conduction in the thickness of the fluid.

This regime can be obtained if the height to thickness ratio (L/e) or extension of the cell is sufficiently large to uncouple conductive and convective heat transfer. The question is to know how a cell with a large enough extension, as indicated by a parameter that can serve as an efficient criterion, can help with this task.

For the case of a cell with an infinite extension, we can show that speed and temperature fields are theoretically uncoupled but, in practice, the cell extension always maintains a finite value.

Thus, the case of a cell with a finite extension should be investigated. This study will be carried out with numerical codes that will be first validated using benchmark results in well-known configurations in the literature before it is used in the transient regime for closed squares and large cavities with natural convection subjected either to a temperature step or to a heat impulse stimulation.

2.1. Analytical One-Dimensional (1D) Approach

At first, we are interested in free convection flow between two infinite slabs subjected to thermally uniform boundary conditions (see Fig. 1). We usually make the Boussinesq assumption. The fluid is considered to be viscous and incompressible.

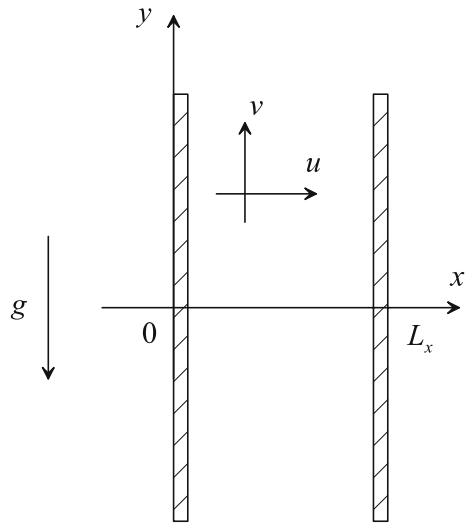

Fig. 1. Cell with an infinite extension.

The corresponding governing equations are:

- Mass conservation:

$$\frac{\partial \rho}{\partial t} + \rho\left(\frac{\partial u}{\partial x} + \frac{\partial v}{\partial y}\right) = 0 \tag{1}$$

- Momentum conservation:

$$\rho\left(\frac{\partial u}{\partial t} + u\frac{\partial u}{\partial x} + v\frac{\partial u}{\partial y}\right) = -\frac{\partial P}{\partial x} + \mu\left(\frac{\partial^2 u}{\partial x^2} + \frac{\partial^2 u}{\partial y^2}\right) \tag{2}$$

and

$$\rho\left(\frac{\partial v}{\partial t} + u\frac{\partial v}{\partial x} + v\frac{\partial v}{\partial y}\right) = -\frac{\partial P}{\partial y} + \mu\left(\frac{\partial^2 v}{\partial x^2} + \frac{\partial^2 v}{\partial y^2}\right) - \rho g \tag{3}$$

- Energy conservation:

$$\rho C\left(\frac{\partial T}{\partial t} + u\frac{\partial T}{\partial x} + v\frac{\partial T}{\partial y}\right) = \lambda\left(\frac{\partial^2 T}{\partial x^2} + \frac{\partial^2 T}{\partial y^2}\right). \tag{4}$$

The cell being of an infinite extension and assuming boundary conditions as uniform, the flow is thus established in the y-direction, that is, $\frac{\partial}{\partial y} = 0$. The conservation equation is reduced to

$$\frac{\partial u}{\partial x} = 0. \tag{5}$$

Moreover, as $\frac{\partial u}{\partial y}=0$, and assuming the adherence of fluid on walls ($u=0$), the heat equation becomes

$$\rho C\frac{\partial T}{\partial t}=\lambda\frac{\partial^2 T}{\partial x^2}. \tag{6}$$

We find the commonly 1D and purely conductive heat transfer transient equation. This is what we call the "pseudo-conduction" regime. It remains to define a criterion for knowing which value of the cell extension will allow us to obtain this regime.

2.2. Numerical 2D Approach in Steady-State Regime

Before dealing with the transient problem, it is necessary, on the one hand, to validate the numerical code we used (Fluent in our case) and, on the other hand, to define a critical Rayleigh number that will allow us to know if we are considered to be in a pseudo-conduction regime. For that, we can refer to several references [1–9] concerning the classical benchmark problem in the steady-state regime of a square cavity heated differentially. The problem can be represented as shown in Fig. 2.

The gravity field g is vertical and downward and the Boussinesq approximation is assumed, that is, the density is independent of the temperature, except in the momentum equation;

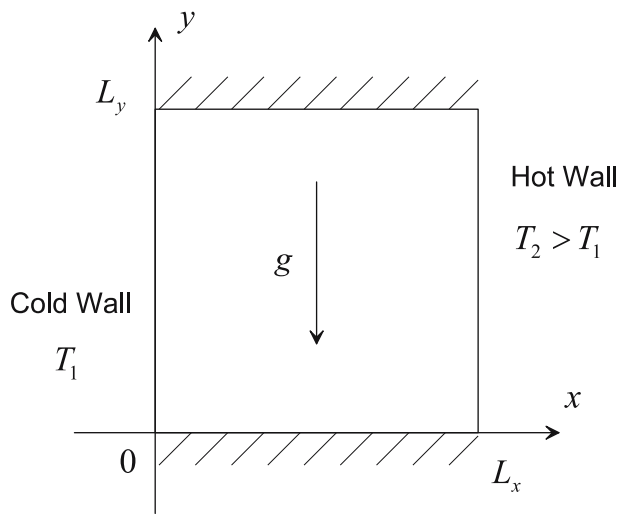

Fig. 2. Square cavity in steady-state regime.

$$\rho = \rho_{\mathrm{m}} \left[1 - \beta \left(T - T_{\mathrm{m}}\right)\right]. \tag{7}$$

The resulting system is the same as the previous one, setting $\frac{\partial}{\partial t} = 0$ (steady-state regime).

Introducing the following reduced quantities:

$$x^* = \frac{x}{L_x}, \quad y^* = \frac{y}{L_y}, \quad u^* = \frac{uL_x}{a}, \quad v^* = \frac{vL_x}{a}, \tag{8}$$

$$p^* = \frac{pL_x^2}{\rho a^2}, \quad T^* = \frac{T - T_1}{T_2 - T_1}, \quad \mathrm{Pr} = \frac{\nu}{a}, \quad Ra = \frac{g\beta \Delta T L_x^3}{\nu a} \tag{9}$$

the equations become

$$\frac{\partial u^*}{\partial x^*} + \frac{\partial v^*}{\partial y^*} = 0 \tag{10}$$

$$u^* \frac{\partial u^*}{\partial x^*} + v^* \frac{\partial u^*}{\partial y^*} = -\frac{\partial p^*}{\partial x^*} + \mathrm{Pr}\left(\frac{\partial^2 u^*}{\partial x^{*2}} + \frac{\partial^2 u^*}{\partial y^{*2}}\right) \tag{11}$$

$$u^* \frac{\partial v^*}{\partial x^*} + v^* \frac{\partial v^*}{\partial y^*} = -\frac{\partial p^*}{\partial y^*} + \mathrm{Pr}\left(\frac{\partial^2 v^*}{\partial x^{*2}} + \frac{\partial^2 v^*}{\partial y^{*2}}\right) + Ra\mathrm{Pr}T^* \tag{12}$$

$$u^* \frac{\partial T^*}{\partial x^*} + v^* \frac{\partial T^*}{\partial y^*} = \frac{\partial^2 T^*}{\partial x^{*2}} + \frac{\partial^2 T^*}{\partial y^{*2}} \tag{13}$$

with the following boundary conditions:

$$\text{in } x^* = 0 \begin{cases} T^* = 0 \\ u^* = v^* = 0 \text{ (adherence to the wall)} \end{cases} \tag{14}$$

$$\text{in } x^* = 1 \begin{cases} T^* = 1 \\ u^* = v^* = 0 \text{ (adherence to the wall)} \end{cases} \tag{15}$$

$$\text{in } y^* = 0 \begin{cases} \frac{\partial T^*}{\partial n} = 0 & \text{(null flux to the wall)} \\ u^* = v^* = 0 & \text{(adherence to the wall)} \end{cases} \tag{16}$$

$$\text{in } y^* = 1 \begin{cases} \frac{\partial T^*}{\partial n} = 0 & \text{(null flux to the wall)} \\ u^* = v^* = 0 & \text{(adherence to the wall).} \end{cases} \tag{17}$$

The fluid is assumed to be viscous and incompressible. Let us consider a 4-mm ×4-mm square cell subjected to a temperature difference ΔT of 10 K with a cold temperature of 300 K and a pressure of 101 325 Pa (atmospheric pressure). (In the next discussion, L_y is increasing by keeping L_x constant). Table I gives the properties for water and oil (Grashoff and Rayleigh numbers are defined, as usual, with respect to the characteristic length L_x);

$$Ra = \frac{g\beta \Delta T L_x^3}{va} = Gr\,\mathrm{Pr}. \tag{18}$$

We note that for the same geometry and the same temperature difference, the Rayleigh number strongly varies according to the fluid. The worst case corresponds to water.

2.2.1. Validation of the Numerical Code

We use the commercial computational fluid dynamics (CFD) code Fluent with a boundary layer type mesh near the boundaries and composed of 80×80 cells. The first validations consist of variations of the number of cells and comparisons of the speed profiles symmetry and energy balance between the inlet and outlet of the system. The last check consists of comparisons between the Nusselt numbers for the front and back faces (top and bottom of the cell are insulated).

$$\phi = hL_y\,(T_2 - T_1) = \int_0^{L_y} \left(-\lambda \frac{\partial T}{\partial x} + \rho c u T\right) dy \tag{19}$$

Table I. Properties for Different Fluids

	Water	Oil	
λ	0.6	0.145	$(\mathrm{W{\cdot}m^{-1}{\cdot}K^{-1}})$
C_1	4182	1880	$(\mathrm{J{\cdot}kg^{-1}{\cdot}K^{-1}})$
μ	0.001	0.8	$(\mathrm{kg{\cdot}m^{-1}{\cdot}s^{-1}})$
ρ	998.2	888	$(\mathrm{kg{\cdot}m^{-3}})$
ΔT	10	10	(K)
β	0.0003	0.0007	$(\mathrm{K^{-1}})$
L_x	0.004	0.004	(m)
L_y	0.004	0.004	(m)
Pr	6.97	10372	–
Gr	1876	0.00541	–
Ra	13080	56.17	–

By definition,

$$Nu = \frac{hL_x}{\lambda} = \frac{\phi L_x}{(T_2 - T_1)\, L_y \lambda}. \tag{20}$$

It yields

$$Nu = \int_0^1 \left(-\frac{\partial T}{\partial x} \frac{L_x}{T_2 - T_1} + \rho c u T \frac{L_x}{\lambda (T_2 - T_1)} \right) d\left(\frac{y}{L_y} \right). \tag{21}$$

In reduced quantities:

$$Nu = \int_0^1 \left(-\frac{\partial T^*}{\partial x^*} + u^* T^* + u^* \frac{T_1}{T_2 - T_1} \right) \mathrm{d}y^*. \tag{22}$$

At the boundaries where $u^* = 0$, the preceding expression is reduced to

$$Nu = \int_0^1 -\frac{\partial T^*}{\partial x^*} \, \mathrm{d}y^*. \tag{23}$$

Table II gives a comparison of the Nu number between the front and back faces. To complete this validation, our results have also been compared with those obtained in a benchmark and especially with the results given by de Walh Davis [1] and Wan et al. [3]. The comparison is carried out with horizontal and vertical maximum speeds and with Nusselt numbers (the Prandtl number is fixed at 0.7). Tables III–V show that our results are consistent.

2.2.2. Results for a Square Cavity

The curves given in Fig. 3 show the results obtained by simulations and those given by correlations [4] for a square cavity. Note the cross dots (our results obtained by Fluent) and circle dots (results obtained in our laboratory by a Galerkine type integral method). In logarithmic space, the asymptotic convection regime results in a linear variation of the Nusselt number with the Rayleigh number. As the Rayleigh number decreases to zero, the Nusselt number is going to unity (purely conductive transfer).

Table II. Comparison of *Nu* Numbers Between the Front and Back Faces

Ra	*Nu*(Front face)	*Nu*(Back face)	Difference	*Nu*(First cell)	*Nu*(Third cell)	Difference
10^3	1.1353	1.1293	0.53%	1.1358	1.1353	0.04%
10^4	2.2547	2.2540	0.03%	2.2552	2.2547	0.02%

Table III. Comparison of Horizontal Maximum Speeds for $x^* = 0.5$

Ra	de Wahl Davis [1]	Wan et al. [3]	Difference between [1] and [3]	Fluent	Difference between Fluent and [1]	Difference between Fluent and [3]
10^3	3.634 (0.813)	3.6434 (0.8167)	0.26%	3.6106 (0.8158)	−0.64%	−0.90%
10^4	16.2 (0.823)	15.967 (0.8167)	−1.44%	16.4088 (0.8158)	1.23%	2.71%
10^5	34.81 (0.851)	33.51 (0.85)	−3.73%	36.737 (0.8406)	5.54%	9.63%

Table IV. Comparison of Vertical Maximum Speeds for $y^* = 0.5$

Ra	de Wahl Davis [1]	Wan et al. [3]	Difference between [1] and [3]	Fluent	Difference between Fluent and [1]	Difference between Fluent and [3]
10^3	3.679 (0.179)	3.686 (0.188)	0.19%	3.6443 (0.1858)	−0.94%	−1.13%
10^4	19.51 (0.12)	19.98 (0.117)	2.35%	19.8609 (0.1233)	1.80%	−0.60%
10^5	68.22 (0.066)	70.81 (0.07)	3.80%	74.2511 (0.0723)	9.69%	4.26%

Table V. Comparison of Nu Numbers

Ra	de Wahl Davis [1]	Wan et al. [3]	Difference between [1] and [3]	Fluent	Difference between Fluent and [1]	Difference between Fluent and [3]
10^3	1.12	1.073	−4.20%	1.1353	1.37%	5.81%
10^4	2.243	2.155	−3.92%	2.2547	0.52%	4.63%

The transition Rayleigh number is usually fixed in the literature to 10^3. If we define the transition by taking the intercept of the line defined from the asymptotic convection regime with the value $Nu = 1$, we obtain almost the same result. However, we observe that the Nusselt number is slightly larger than unity for this value. This means that the temperature field is already affected by the velocity field. That is the reason why Batchelor [5] preferred to set the Ra_c value to 500. In this study a value of 200 is assumed.

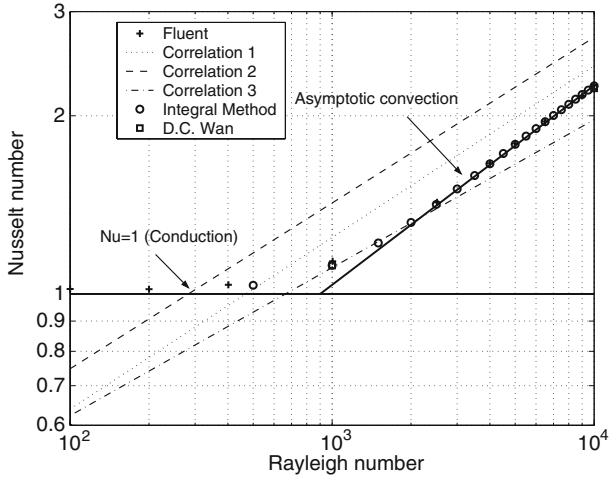

Correlation 1: $Nu = 0.18*(Pr*(Ra/(0.2 + Pr)))^{0.29}$
Correlation 2: $Nu = 0.22*(Pr*(Ra/(0.2+Pr)))^{0.28}$
Correlation 3: $Nu = 0.197*(Ra)0.25$

Fig. 3. Comparisons between the results obtained in this work with other correlations.

2.2.3. Results for a Large Cavity

In this section, the variation of the critical Rayleigh number with the cell extension is considered [5–9] (see Fig. 4).

For a given Rayleigh number, we notice a decrease of the Nusselt number for an extension larger than four. Thus, the effect of convection on heat transfer is reduced for larger cavities (we can note that this variation is nonuniform and that for a smaller extension, for example, an extension of two, the Nusselt number is increasing). In Fig. 5, we have plotted the variation of the critical Rayleigh number with the cell extension. For a value larger than ten, we find a linear variation for the critical Rayleigh number that leads to

$$Ra_c = 200\, Al \quad (Al > 10) \tag{24}$$

(to be compared with the Batchelor criterion: $Ra_c = 500\, Al$).

As the curve $Ra_c = f(Al)$ is linear, a new definition for the Rayleigh number valid for extensions can be proposed:

$$Ra^* = \frac{g\beta \Delta T L_x^2 L_y}{va}. \tag{25}$$

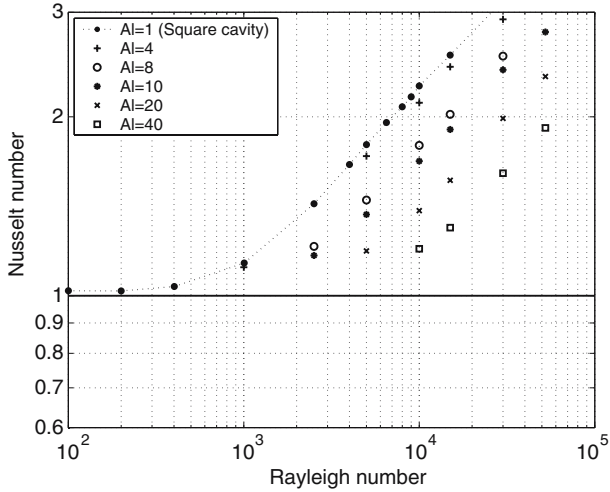

Fig. 4. $Nu = \mathrm{f}(Ra)$ for different extensions.

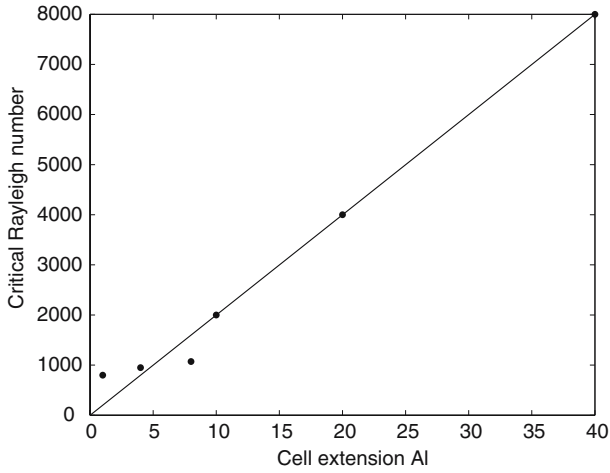

Fig. 5. Critical Rayleigh number vs. cell extension.

We obtain

$$Ra_c^* = 200. \tag{26}$$

(For this correlation, the Prandtl number is equal to 0.7. As the Prandtl number is increasing with the fluid viscosity, this corresponds to the worst case.)

2.3. Natural Convection in Transient Regime

Few studies have been carried out in the transient regime and particularly in the impulse regime. We can note, for instance, Refs. 10 and 11, which are interesting in the establishment of speed and temperature fields in a cavity heated differentially (the temperature of the cavity is assumed as uniform at the initial time).

However, this kind of problem is far from our experiment. In our case, the back face is nearly adiabatic while the front face is subjected to a short heat pulse in time. As ΔT is a function of time (it is maximum for smaller times and goes to zero at larger times), the main difficulty is to know which temperature must be considered for calculating the Rayleigh number.

The problem is thus to evaluate $\Delta T_{\max}$. In our experiment, the adiabatic temperature for the fluid is low and is about 1 K, but this is not the case for the temperature of the metallic wall in the front face that is increasing very quickly at an initial time. This temperature (T_i) can be calculated from this relation:

$$Q/S = \rho c_w e_w T_i \tag{27}$$

The adiabatic temperature is then given by

$$Q/S = (2\rho c_w e_w + \rho c_l e_l)\, T_l. \tag{28}$$

Thus,

$$T_i = \frac{(2\rho c_w e_w + \rho c_l e_l)}{\rho c_w e_w} T_l \tag{29}$$

For water with $e_w = 1$ mm and $e_l = 4$ mm, we obtain: $T_i \simeq 7$ K.

Using the critical Rayleigh number defined in Eq. (24), the critical cell extension for water is given by $Al_c = 45$ (from the Batchelor criterion, $Al_c = 18$). In practice, our measuring cell exhibits an extension of 25, which could be critical for water but large enough for other fluids.

We have now to study the case of a transient regime. For this case a temperature step that is easier to simulate is first considered and will be then used for validation of the more realistic case of the impulse heat flux stimulation.

2.3.1. Cavity Subjected to a Temperature Step

The first case corresponds to a cell insulated on the back face and subjected to a temperature step on the front face. For this case, the CFD code (Fluent) allows us to compute the temperature response of the back

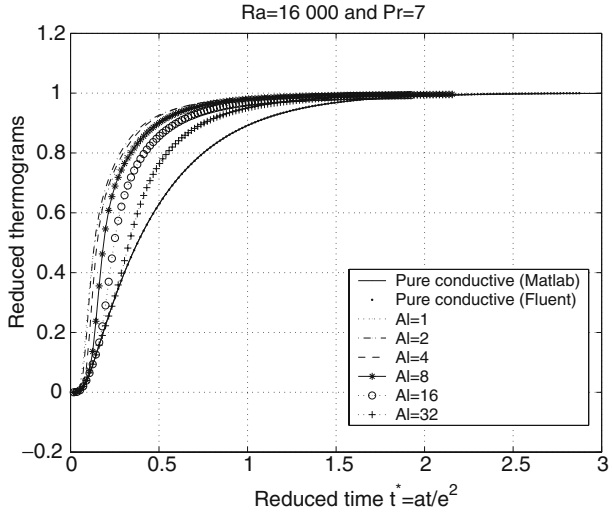

Fig. 6. Rear-face thermograms for different cell extensions.

face up to a Rayleigh number of 16,000 (see Fig. 6). The results show that it is not possible to obtain purely conductive heat transfer ($\mathrm{Pr} = 7$ and $Ra = 16,000$) for an extension fewer than 32. In contrast, for a Rayleigh number of 1600, we can show that an extension of 16 is large enough.

The criterion obtained in the steady-state regime leads to similar results as those obtained in the transient regime (at first sight, it was not so obvious), that is, an extension of 80 for a Rayleigh number of 16,000 and 8 for $Ra = 1600$.

2.3.2. Cavity Subjected to Heat-Pulse Stimulation

The case of a Dirac delta function of flux (impulse stimulation) is not only more realistic but also a more difficult case to solve numerically because the deposition of energy on the front face occurs in a very short duration. The temperature within the medium continuously varies with time to reach a uniform temperature at larger times corresponding to the adiabatic temperature of the system. The driving term (natural convection) is larger for the early times and is rapidly disappearing with a decrease of the temperature difference between the front and back faces.

This problem is difficult to solve with Fluent because it requires very small time steps at the beginning (approximately $\Delta t^* = 10^{-6}$). To overcome this difficulty, we have to use another computational code FlexPde, which allows us to obtain good results from its in-time and in-space adaptive

mesh. To validate the use of this code, we proceed to a cross-comparison between the results given by this code and those given by Fluent for the previous case of a temperature step stimulation (see Fig. 7).

Then, the back-face response in the middle of the cell and for different extensions have been simulated by FlexPDE for the case of a heat-pulse stimulation.

For this case, the Rayleigh number is defined from the adiabatic temperature of the sample, which is equal to 1000 for the case of water. The results are shown in Fig. 8. We can observe that for an extension larger than 16, the thermogram is purely conductive.

2.4. End Effects in the Measuring Cell

As explained in the first part (Part I) of this work in the implementation of the experimental bench, the measuring cell is composed of two metallic cylinders separated by an insulating material (Teflon®) to avoid thermal shorts between the inner and outer cylinders (end effects). The temperature measurement is performed in the middle of the cell.

An explanation of these technical choices is derived from a numerical study we performed that takes into account both the coupled conduction and convection in the fluid and the conduction through the metallic walls. For the case of insulating walls, we can show that free convection is emphasized. The in-time response or thermogram goes faster at the top of

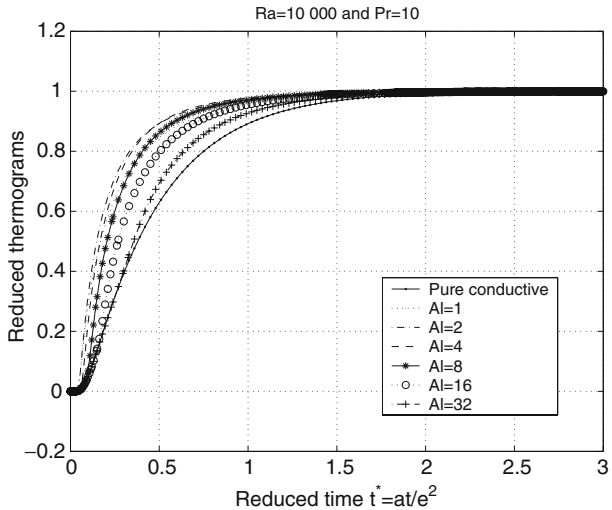

Fig. 7. FlexPDE simulations for the case of a temperature step ($\Delta T = 10\,\mathrm{K}$).

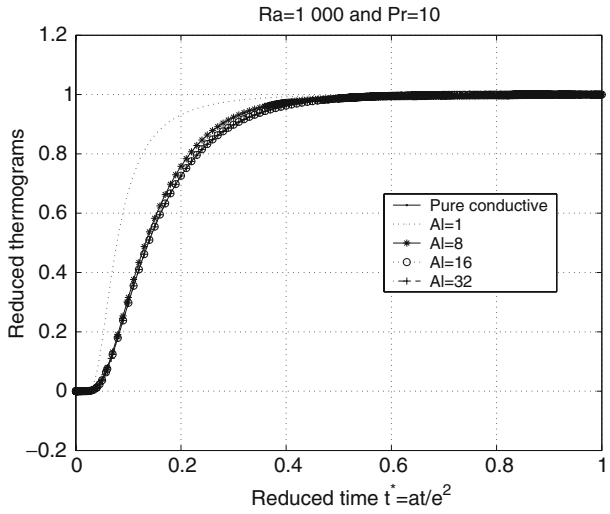

Fig. 8. FlexPDE simulations for the case of a heat-pulse stimulation (Dirac function).

the cell and slower at the bottom, while the thermogram measured in the middle of the cell is as close as possible to the purely conductive thermogram. That is the reason why the temperature is measured at this location in the experiments. Conversely, conducting materials can be used to limit convection in decreasing the temperature gradient in the vertical direction of the cylinders but if discrepancies between thermograms are less, they are also more sensitive to end effects in this case. So, it clearly appears that there exists an optimum value for the wall conductivity, which is represented by stainless steel, which allows us to eliminate the end effects and the influence of convection.

2.5. Conclusion

We have shown through this numerical study the interest to precisely model the coupled conductive–convective transfer. If it is easy to show that conduction is uncoupled with convection for the case of a cell with an infinite extension, we have shown that, in practice, it is difficult to fulfil this condition.

We have also focused on the interest to consider, in the simulations, some boundary conditions as close as possible to the experiment (impulse stimulation). Indeed, the criteria proposed in the literature, which are obtained in most cases in a steady-state regime, can strongly differ from one author to the other and can lead to differences of a factor larger

than two in the cell dimensions. This can be mainly explained by the difficulty in determining accurately the transition region between the asymptotic pseudo-conduction regime and the asymptotic convection. Another result is derived from the criteria obtained in the steady-state regime that cannot be extended to the transitory regime and that also depend on the boundary conditions of the system (imposed temperatures or Dirac heat flux). Finally, we have determined that the Rayleigh number cannot be defined in the same way in steady-state and transient regimes.

The main result is that, for the case of the more constraining liquid that is water and for the case of the flash method, an extension of 16 is large enough to result in purely conductive heat transfer.

3. RADIATIVE HEAT TRANSFER

In the preceding part, we were interested in the conduction–convection coupling. We have shown how it was possible to eliminate convection by a judicious choice of the cell geometry (large extension) and of the measurement conditions (small temperature variations). To perform such a measurement at high temperatures with a similar device, the conduction–radiation coupling must also be considered but it is not exactly the same for radiation as for convection. Indeed, even if it is possible to reduce its effects using some reflecting walls, it cannot be totally removed from heat transfer. The only possible solution is to develop an adapted model, which can take into account the coupled conductive–radiative heat transfer.

If the distance between the two inner cylinders is small compared to their radii, the configuration factors, which are used to evaluate the net flux exchanged between the inner walls of the measuring cell are exactly the same as those obtained between two infinite slabs.

In the same way as for conduction and convection, we then can use the Cartesian coordinates system for solving the radiative transfer equation (RTE).

The conductive–radiative equations are usually difficult to solve due to the strong coupling that exists between the heat transfer equation where the divergence of the radiative flux appears as a source term (Eq. (31)) and the RTE (Eq. (30)) that is a function of the temperature field through the blackbody emission term. In simple geometrical configurations such as heat transfer between two parallel and infinite slabs, the problem can be simplified and solved analytically. We propose here an approximate solution for this problem that gives quite satisfactory results in most cases. In other cases, a more sophisticated model can be used [12–14].

3.1. General Equations

We have two conservative equations, one based on the intensity and the other on the temperature:

- Radiative transfer equation:

$$\frac{dI_\nu}{ds} + (K_\nu + \sigma_\nu) I_\nu = K_\nu n^2 I_\nu^0 (T) + \frac{\sigma_\nu}{4\pi} \int_{4\pi} P\left(\Delta' \to \Delta\right) I_\nu \left(\Delta', s\right) d\Omega' \tag{30}$$

with $I_\nu^0 (T)$: blackbody intensity in vacuum, I_ν: monochromatic intensity (see Fig. 9), K_ν: monochromatic absorption coefficient, σ_ν: monochromatic scattering coefficient, n: refractive index of the material.

Let us introduce

$\beta_\nu = K_\nu + \sigma_\nu$: monochromatic extinction coefficient
$\omega_\nu = \sigma_\nu / \beta_\nu$: "Albedo"

- Energy equation:

$$\rho c \frac{\partial T}{\partial t} = -\mathrm{div}\,(\vec{\varphi}_c + \vec{\varphi}_r) \tag{31}$$

with:

$$\vec{\varphi}_c = -\lambda \overrightarrow{\mathrm{grad}}\,(T) \tag{32}$$

and

$$\vec{\varphi}_r = \int_0^\infty \int_{4\pi} I_\nu (\Delta, s)\, \vec{n}.\vec{u}\, d\Omega . d\nu. \tag{33}$$

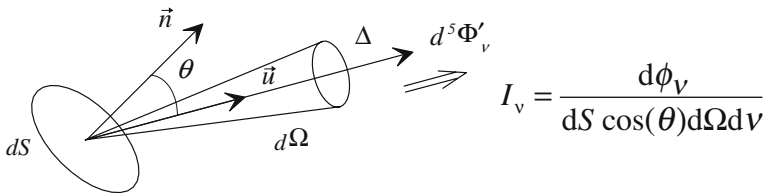

Fig. 9. Definition of the intensity I_ν.

3.2. Simplification of the Problem

The case we consider here can be modelled by an infinite slab with a thickness e, allowing us to assume

- one-dimensional heat transfer
- azimuthal symmetry

Thus, the intensity is only a function of the variables z and θ (see Fig. 10). Setting $\mu = \cos(\theta)$, RTE becomes

$$\frac{\mu}{\beta_\nu}\frac{dI_\nu}{dz} + I_\nu = (1-\omega_\nu)\, I_\nu^0(T) + \frac{\omega_\nu}{2}\int_{-1}^{+1} p\left(\mu' \to \mu\right)\, I_\nu\left(\mu', z\right)\, d\mu' \tag{34}$$

with

$$\varphi_r(z) = \int_0^\infty 2\pi \int_{-1}^{+1} I_\nu(z,\mu)\,\mu\, d\mu\, d\nu \tag{35}$$

and the energy equation becomes

$$\frac{\partial^2 T}{\partial z^2} - \frac{1}{\lambda}\frac{\partial \varphi_r}{\partial z} = \frac{1}{a}\frac{\partial T}{\partial t}. \tag{36}$$

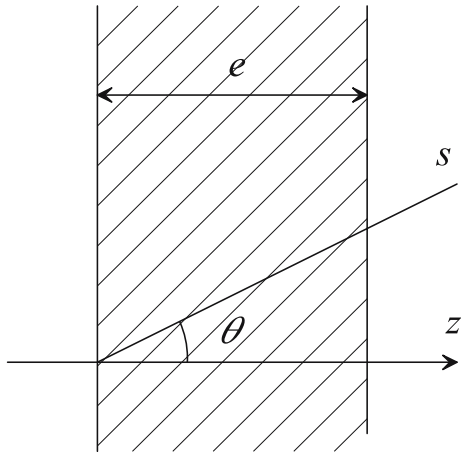

Fig. 10. Projection of the RTE.

3.3. Notion of Radiative Conductivity

As the boundaries of a semi-transparent material are opaque, which is the case here, the conductive–radiative coupling can be modelled by a simple thermal resistance. The expression for this resistance can differ with the extinction coefficient of the material (or more precisely with its optical thickness). For instance, for the case of a highly absorbing material, the effect of the boundaries can be neglected compared to the absorption phenomena in the material. In this case, the radiative transfer can be viewed like a pure diffusion process and can be modelled by a simple resistance $R_r = e/\lambda_r$ (λ_r is the radiative conductivity). In the literature, this model is known as Rosseland's model. The opposite case corresponds to a low absorbing medium (thin film). In this case, the radiative heat transfer can also be represented by a simple resistance but with another expression; conduction and radiation are uncoupled in the medium but stay linked through the boundary conditions.

In all cases, the quadrupole model can be set-up very quickly and keep the same formulation.

Since the total heat flux ϕ is the sum of the conductive and radiative fluxes, the conductive–radiative transfer can be modelled by a conductive quadrupole and a radiative quadrupole in parallel (See Fig. 11). In our case, the radiative quadrupole is a purely resistive quadrupole:

$$M_r = \begin{bmatrix} A_r = 1 & B_r = R_r = e/\lambda_r \\ C_r = 0 & D_r = 1 \end{bmatrix}. \tag{37}$$

The equivalent quadrupole is then given by

$$M' = \begin{bmatrix} A' = \frac{AR_r + B}{B + R_r} & B' = \frac{BR_r}{B + R_r} \\ C' = \frac{CR_r + D + A - 2}{B + R_r} & D' = \frac{B + R_r D}{B + R_r} \end{bmatrix}. \tag{38}$$

It can be used in a similar way as the purely conductive quadrupole. Depending on the optical thickness of the material, several authors [15–19] have proposed different expressions for λ_r:

- Low optical thickness, $\tau_0 << 1$ (grey medium, grey and scattering boundaries):

$$\lambda_r = \frac{4n^2\sigma\overline{T}^3 e}{\frac{1}{\varepsilon_1} + \frac{1}{\varepsilon_2} - 1} \tag{39}$$

- Rosseland's model, $\tau_0 >> 1$ (grey medium):

$$\lambda_r = \frac{16}{3} n^2 \sigma \frac{\overline{T}^3}{\beta} \tag{40}$$

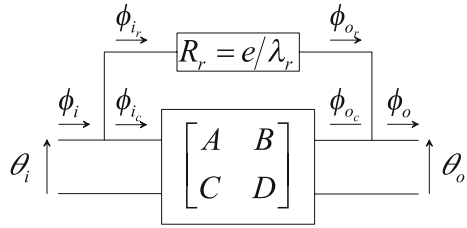

Fig. 11. Conductive–radiative quadrupole model for fluid.

- Poltz-Jugel's model, $\tau_0 \simeq 1$ (grey medium, grey and scattering boundaries):

$$\lambda_r = \frac{16}{3} n^2 \sigma \frac{\overline{T}^3}{\beta} Y \quad \text{with} \quad Y = 1 - \frac{3}{4\tau_0}(1 - 4E_5(\tau_0)) - \frac{2}{3\tau_0} \frac{(1-(\varepsilon_1+\varepsilon_2)/2-2\rho_1\rho_2 E_3(\tau_0))}{1-4\rho_1\rho_2 E_3(\tau_0)^2} (1 - 3E_4(\tau_0))^2 \tag{41}$$

  (as $\tau_0 \to \infty$, Rosseland's model is found $Y \to 1$, and as $\tau_0 \to 0$, the thin film model is found)

- Radiative equilibrium model (grey medium, grey and scattering boundaries):

$$\lambda_r = \frac{4n^2 \sigma \overline{T}^3 e}{\frac{1}{\varepsilon_1} + \frac{1}{\varepsilon_2} - 1 + \beta e} \tag{42}$$

- Dessler's model (grey medium, grey and scattering boundaries):

$$\lambda_r = \frac{4n^2 \sigma \overline{T}^3 e}{\frac{1}{\varepsilon_1} + \frac{1}{\varepsilon_2} - 1 + \frac{3}{4}\beta e} \tag{43}$$

- Modified radiative equilibrium model (grey medium, grey and scattering boundaries):

$$\lambda_r = \frac{4n^2 \sigma \overline{T}^3 e}{\frac{1}{\varepsilon_1} + \frac{1}{\varepsilon_2} - 1 + \frac{\beta e}{K}} \tag{44}$$

with $K(\beta e) = 4/3 - 0.175 \exp(-0.56865 \beta e) - (1/3 - 0.175) \exp(-5.6114 \beta e)$.

The preceding models are of interest for estimation of the conductive properties of semi-transparent fluids with low absorption coefficients at infrared wavelengths or measurements at high temperatures. This can be done easily through this model in introducing only one additional parameter, the radiative resistance R_r. Figure 12 gives an example of thermograms we can obtain as a function of the radiative resistance R_r for a case of a measuring cell with copper walls. We can observe that the effect of this parameter on the thermogram appears at smaller times, which allows us to think that this parameter is independent of the thermal diffusivity and thermal conductivity. Keeping an analytical approach, this radiative model can be improved by the introduction of two new parameters (the optical thickness and the Planck number of the semi-transparent material). More details can be viewed in Refs. 12–14.

4. CONCLUSION

We have shown in this second part (Part II) how we can, by a judicious choice of the measuring cell extension, remove the effects of natural convection and how it is possible to take into account the radiative effects in a very simple way for semi-transparent liquids through an additional parameter, the radiative resistance. Using such a model, an extension to

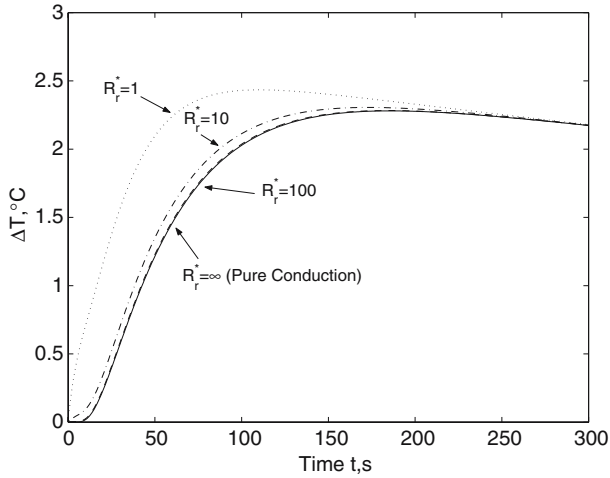

Fluid [e_f =4 mm, λ_f= 0.2 W·m^{-1}·K^{-1}, a_f = 1× 10^{-7} m^2·s^{-1},ρc_f = 2 ×10^6 J·m^{-3}·K^{-1}]
Walls (Copper) [e_w = 1 mm, λ_w= 395 W·m^{-1}·K^{-1}, a_w = 1.15× 10^{-4} m^2·s^{-1},ρc_w = 3.43× 10^6 J·m^{-3}·K^{-1}]
h = 5 W·m^{-2}·K^{-1}, Q/S = 4 × 10^4 J·m^{-2}

Fig. 12. Thermograms for different values of $R_r^* = R_r / R_{cd}$ $(R_{cd} = e_l / \lambda_l)$.

higher temperatures (up to 500°C) of the experiment presented in the first part (Part I) of this work is possible by keeping the same configuration.

ACKNOWLEDGMENT

We would like to thank the Bureau National de Métrologie (Paris) for its financial support (Contract BNM-INPL No. 023001).

REFERENCES

1. G. de Wahl Davis, *Int. J. Numer. Methods Fluids* **3**:249 (1983).
2. G. de Wahl Davis and I. P. Jones, *Int. J. Numer. Methods Fluids* **3**:227 (1983).
3. D. C. Wan, B. S. V. Patnaik, and G. W. Wei, *Numer. Heat Transfer, Part B* **40**:199 (2001).
4. F. P. Incropera and D. P. DeWitt, *Fundamentals of Heat and Mass Transfer* (Wiley, New York, 1996).
5. G. K. Batchelor, *Q. Appl. Math.* **12**:209 (1953).
6. H. Manz, *Energy Build* **35**:305 (2003).
7. J. L. Wright, *ASHRAE Trans.* **106**:940 (1996).
8. S. H. Yin, T. Y. Wung, and K. Chen, *Int. J. Heat Mass Transfer* **21**:307 (1978).
9. D. Misra and A. Sarka, *Comp. Methods Appl. Mech. Eng.* **141**:205 (1997).
10. J. Patterson and J. Imberger, *J. Fluid Mech.* **100**:65 (1980).
11. M. A. Leal, H. A. Machado, and R. M. Cotta, *Int. J. Heat Mass Transfer* **43**:3977 (2000).
12. S. André and A. Degiovanni, *Int. J. Heat Mass Transfer* **38**:3401 (1995).
13. S. André and A. Degiovanni, in *Proc. 2nd Eur. Thermal-Sciences and 14th UIT Nat. Heat Transfer Conf.*, Vol. 3, G. P. Celata, P. Di Marco, and A. Mariani, eds. (ISBN: 88-7741-911-3, 1996), pp. 1441–1447.
14. S. André and A. Degiovanni, *J. Heat Transfer* **120**:1 (1998).
15. A. Schuster, *J. Astrophys.* **21**:1 (1905).
16. B. K. Larkin, *A Study of the Rate of Thermal Radiation Through Porous Insulating Materials*, Ph. D. Thesis (University of Michigan, Ann Arbor, Michigan, 1957).
17. H. C. Hamaker, *Philips Res. Rept.* (1947).
18. H. Poltz and R. Jugel, *Int. J. Heat Mass Transfer* **10**:1075 (1967).
19. R. G. Dessler, *J. Heat Mass Transfer* **86C**:240 (1967).